NANO · MICRO small

www.small-journal.com

Engineering Morphologies of Cobalt Pyrophosphates Nanostructures toward Greatly Enhanced Electrocatalytic Performance of Oxygen Evolution Reaction

Hongfang Du, Wei Ai, Zhi Liang Zhao, Yu Chen, Xin Xu, Chenji Zou, Lishu Wu, Lan Su, Kaikai Nan, Ting Yu, and Chang Ming Li**

Herein, a surfactant- and additive-free strategy is developed for morphology-controllable synthesis of cobalt pyrophosphate (CoPPi) nanostructures by tuning the concentration and ratio of the precursor solutions of $Na_4P_2O_7$ and $Co(CH_3COO)_2$. A series of CoPPi nanostructures including nanowires, nanobelts, nanoleaves, and nanorhombuses are prepared and exhibit very promising electrocatalytic properties toward the oxygen evolution reaction (OER). Acting as both reactant and pseudo-surfactant, the existence of excess $Na_4P_2O_7$ is essential to synthesize CoPPi nanostructures for unique morphologies. Among all CoPPi nanostructures, the CoPPi nanowires catalyst renders the best catalytic performance for OER in alkaline media, achieving a low Tafel slope of 54.1 mV dec^{-1}, a small overpotential of 359 mV at 10 mA cm^{-2}, and superior stability. The electrocatalytic activities of CoPPi nanowires outperform the most reported non-noble metal based catalysts, even better than the benchmark Ir/C (20%) catalyst. The reported synthesis of CoPPi gives guidance for morphology control of transition metal pyrophosphate based nanostructures for a high-performance inexpensive material to replace the noble metal-based OER catalysts.

H. Du, Z. L. Zhao, L. Su, K. Nan, Prof. C. M. Li
Institute for Clean Energy and Advanced Materials
Faculty of Materials and Energy
Southwest University
Chongqing 400715, China
E-mail: ecmli@swu.edu.cn

H. Du, Dr. W. Ai, Y. Chen, Dr. X. Xu, C. Zou, L. Wu, Prof. T. Yu
Division of Physics and Applied Physics
School of Physical and Mathematical Sciences
Nanyang Technological University
Singapore 637371, Singapore
E-mail: yuting@ntu.edu.sg

H. Du, Z. L. Zhao, L. Su, K. Nan, Prof. C. M. Li
Chongqing Key Laboratory for Advanced Materials
and Technologies of Clean Energies
Chongqing 400715, China

Prof. C. M. Li
Institute of Materials Science and Devices
Suzhou University of Science and Technology
Suzhou 215011, China

The ORCID identification number(s) for the author(s) of this article can be found under https://doi.org/10.1002/smll.201801068.

DOI: 10.1002/smll.201801068

Environmental pollution and global warming stemming from the overconsumption of traditional fossil fuels have motivated intensive development of clean and renewable energy sources,[1] for example, hydrogen.[2] Water with a coverage of around 70% of the Earth's surface[3] is the most abundant precursor to be converted into hydrogen via electrolysis, which involves hydrogen evolution reaction (HER) and oxygen evolution reaction (OER).[4] The OER experiences multistep proton-coupled electron transfer, a kinetically and thermodynamically unfavorable process, and generally results in high overpotentials for considerable energy loss during water electrolysis.[5] Thus, electrocatalysts are used to promote the OER process.[6] Noble metal (e.g., Ir and Ru) based materials show high OER catalytic performance;[7] however, the widespread applications are greatly hindered by their scarcity and high cost.[8] Alternatively, non-noble metal electrocatalysts with the ability of large-scale production and low cost have thus been explored,[9] such as Fe, Ni, and Co-based materials.[10] Among them, Co-based materials are the most promising candidates by virtue of their excellent electrocatalytic activities.[11] Up to date, various Co-based materials, including (hydr) oxides,[12] sulfides,[13] phosphides,[14] nitrides,[15] phosphates,[16] etc., have been extensively studied, in which cobalt phosphates (CoPi) are of particular interests because of their unique self-healing property and mild working conditions.[17] Nonetheless, their fascinating OER activities have never been realized until the pioneering work started by Nocera and Kanan, which opens up a new field of Co-based electrocatalysts toward OER applications.[16]

Cobalt pyrophosphate ($Co_2P_2O_7$, CoPPi) is a derivative of CoPi, in which two PO_4^{3-} (phosphate) tetrahedra sharing one oxygen atom to form one $P_2O_7^{4-}$ (pyrophosphate) unit.[18] CoPPi has a layered crystal structure and possesses unique magnetic, optical, and electrical properties,[19] which is expected to be better than CoPi in virtue of its physicochemical structure. Despite its broad applications as electrode materials for batteries[20] and supercapacitors,[20c,21] the OER catalytic activity of CoPPi has been rarely studied. Recently, CoPPi nanocrystals

were constructed as the OER electrocatalyst via sol-gel combined with annealing processes.[19] However, the strategy experiences tedious procedures that are disadvantageous for mass production. On the other hand, due to the high-temperature condition the morphology and nanostructure of the resultant product are greatly damaged to negatively affect electrocatalytic behavior toward OER. This is because that the morphology of nanomaterials often plays a vital role in electrocatalysis, which dominates the reactivity and amount of electroactive sites as well as the mass transport paths.[22] Therefore, engineering of morphology is essential for nanomaterials, and is definitely challenging in the synthesis arts, in particular in morphology-controllable synthesis of CoPPi, and even CoPi.

Herein, we report a newly developed method to synthesize various CoPPi nanostructures, including nanowires, nanobelts, nanoleaves, and nanorhombuses, by simply tuning the concentration and ratio of the two precursors ($Na_4P_2O_7$ and $Co(CH_3COO)_2$). Differently from the previously reported approaches for morphology-controllable synthesis, our methodology does not involve any toxic solvent, surfactant, and additives, and hence is more convenient for mass production because of its safety and simplicity. We discover that the presence of excess $Na_4P_2O_7$ in the solution is beneficial to achieve unique nanostructures of CoPPi. The formation mechanism for CoPPi nanostructures is proposed, and offers great scientific insights for morphology-controllable synthesis of other nanostructured transition metal pyrophosphates. The electrocatalytic properties of various CoPPi are also investigated, among which the nanowires exhibit the best OER performance with a low Tafel slope of 54.1 mV dec^{-1}, a small overpotential of 359 mV at 10 mA cm^{-2}, and superior stability, which outperforms the most reported non-noble metal-based OER catalyst, and is even better than the benchmark Ir/C catalyst.

CoPPi nanowires are prepared by hydrothermal treatment of a mixed solution containing identical volume of 300×10^{-3} M $Na_4P_2O_7$ and 200×10^{-3} M $Co(CH_3COO)_2$ solutions (details are presented in the Supporting Information). Scanning electron microscopy (SEM) image of the as-synthesized material shows a nanowire-like structure with uniform morphology (**Figure 1**a). The size of an individual nanowire is ≈20 nm wide and ≈2 µm long (inset of Figure 1a). Energy-dispersive X-ray (EDS) analysis suggests the presence of Co, P, O, and Na in the nanowires (Figure S1, Supporting Information). The existence of Co, P, and O agrees well with the elemental compositions of $Co_2P_2O_7$, while the signal of Na is probably attributed to the surface absorbed $Na_4P_2O_7$ on CoPPi. However, the amount of $Na_4P_2O_7$ in CoPPi nanostructures is low and Na^+ is inert in anodic reactions. Thus, we believe that the adsorbed $Na_4P_2O_7$ does not affect the OER catalytic activity of CoPPi. The corresponding EDS mapping images suggest that the nanowires are composed of uniformly distributed Co, P, and O (Figure 1b). The strong symmetric vibrations of PO_3 group and POP bridge are observed in Raman spectrum at 1030 and 740 cm^{-1}, respectively, further confirming the existence of pyrophosphate group in CoPPi nanowires (Figure S2, Supporting Information).[23] X-ray diffraction (XRD) pattern of the product illustrates four predominate peaks located at 24.6°, 29.2°, 30.4°, and 36.2° (Figure S3, Supporting Information), which can be assigned to (120), (111), (12), and (040) planes of $Co_2P_2O_7$ (JCPDS No. 87-0457), respectively. Transmission electron microscopy (TEM) observation reveals that the nanowires have a long and thin-flake like structure (Figure 1c,d). The lattice pattern with fringe spacings of 0.256 and 0.216 nm are observed in the high-resolution TEM (HRTEM) image (Figure 1e), attributable to the (210) and (201) planes of $Co_2P_2O_7$, respectively. X-ray photoelectron spectroscopy (XPS) spectrum of the nanowire is shown in Figure S4 (Supporting Information), signals of Co, P, O, and Na are detected, consistent with the results of EDS measurement. High-resolution XPS (HRXPS) spectra of Co 2p, O 1s, and P 2p are measured for further analysis (Figure 1f), in which Co 2p spectrum displays two main peaks located at 780.7 and 797.3 eV corresponding to Co $2p_{3/2}$ and Co $2p_{1/2}$,[24] respectively. This observation indicates that the cobalt presents in +2 oxidation state,[24,25] which is consistent with the theoretical value of $Co_2P_2O_7$. Another two small peaks at 786.4 and 802.8 eV can be sequentially attributed to the satellite peak of Co $2p_{3/2}$ and Co $2p_{1/2}$.[26] HRXPS of O 1s spectrum can be deconvoluted into two peaks (Figure 1g). The one centered at 533.1 eV can be assigned to P—O—P in CoPPi, while another peak at 531.5 eV is related to P=O.[27] In the HRXPS spectrum of P 2p region, a single peak centered at 133.2 eV is observed (Figure 1h), which is attributed to the pyrophosphate group in CoPPi.[28] These results suggest that CoPPi nanowires have been successfully synthesized.

Though a few morphologies of CoPPi nanostructures have been synthesized with different approaches before this work, nanowire-structured CoPPi and even CoPi are never been realized. Generally, synthesis of 1D structured materials requires a rigorous condition. For example, a moderate amount of poly(vinyl pyrrolidone) as capping agent is crucial for preparing Ag nanowire,[29] while organic oleylamine as a stabilizer is indispensable for the synthesis of Au nanowire.[30] Herein, we successfully synthesized CoPPi nanowires with uniform morphology through a facile yet efficient method by mixing two reactants $Na_4P_2O_7$ and $Co(CH_3COO)_2$ without any surfactant and additive. Therefore, the mechanism of such a promising method is expected to be very important for both fundamental understandings and practical applications. Previous work reported that $P_2O_7^{4-}$ can mediate the nanostructure of Pt for its unique coordination properties.[31] We suppose that $Na_4P_2O_7$ also plays a vital role in the formation of CoPPi nanowires in this system. Therefore, we control the concentration and ratio of the two reactants to further study the details.

We first investigated the effects of the precursors' concentration on the formation of CoPPi nanostructures. When both the concentration of $Na_4P_2O_7$ and $Co(CH_3COO)_2$ are lowered to 20% of that for preparing the nanowires (i.e., 60×10^{-3} M $Na_4P_2O_7$ and 40×10^{-3} M $Co(CH_3COO)_2$ solutions), uniform CoPPi nanobelts are obtained. The typical width of the nanobelts is about 300–400 nm with several micrometers in length (**Figure 2**a–c). Further lowering the concentration of the precursors (5% of that for nanowires) could promote the formation of CoPPi nanoleaves with a representative size of ≈1 µm × 3 µm (Figure 2d–f). With a concentration of 2.5% of the original solutions, rhombus-like CoPPi is prepared (Figure 2g–i). The size of the nanorhombuses is ≈3 µm in width and ≈6 µm in height. No CoPPi nanostructures are formed under the extremely low concentration (1% of the original solution). Additionally, the

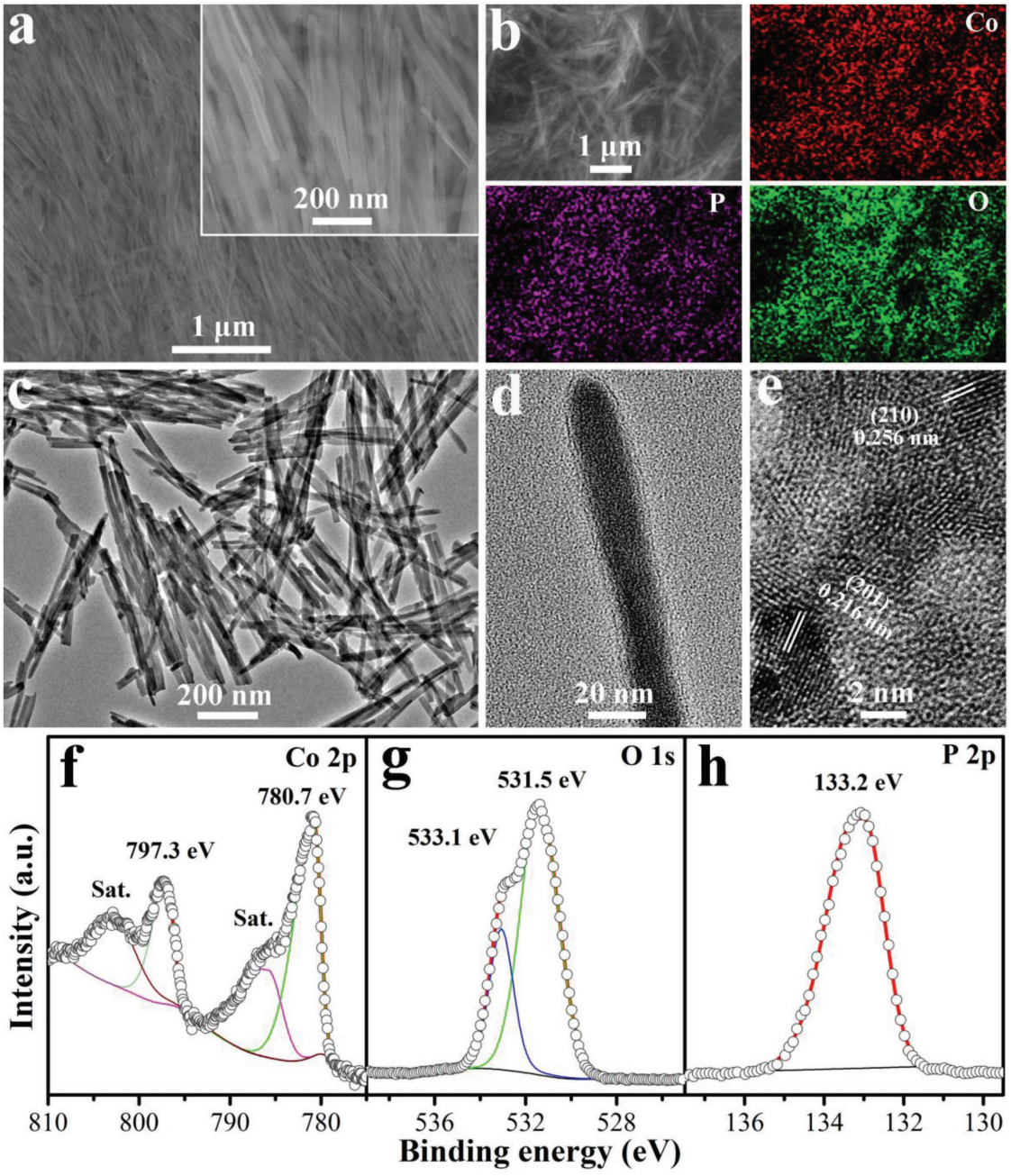

Figure 1. a) SEM and b) EDS mapping images of CoPPi nanowires; c,d) TEM and e) HRTEM images of CoPPi nanowires. HRXPS spectra of CoPPi nanowires in f) Co 2p, g) O 1s, and h) P 2p regions.

coexistence of CoPPi nanowires and nanobelts is observed when the concentration is 50% of that for nanowire (Figure S5a, Supporting Information), and both CoPPi nanobelts and nanoleaves are collected when the concentration is 10% of the original solution (Figure S5b, Supporting Information). The above results clearly indicate the morphology of the final product could be effectively engineered by tuning the concentration of the precursor solutions. The role of precursors' concentration on the controlling morphology of final products is illustrated in **Figure 3**a. According to La-Mer model, higher precursor concentration endows higher supersaturation ratio of monomer CoPPi in solution, which will lead to the formation of large number of nuclei in a short period and the concentration of monomer will drop below the critical nucleation concentration, followed by growth of the nuclei by diffusion of monomer to their surface.[32] Therefore, the high precursor concentration condition prefers to produce small size CoPPi material, that is, nanowires. On the contrary, fewer nuclei can be formed at lower concentration condition and the nuclei are able to grow into more perfect crystal with bigger size, that is, nanorhombuses. It is worthy to note that an overdose of $Na_4P_2O_7$ is present in the solution because the molar ratio

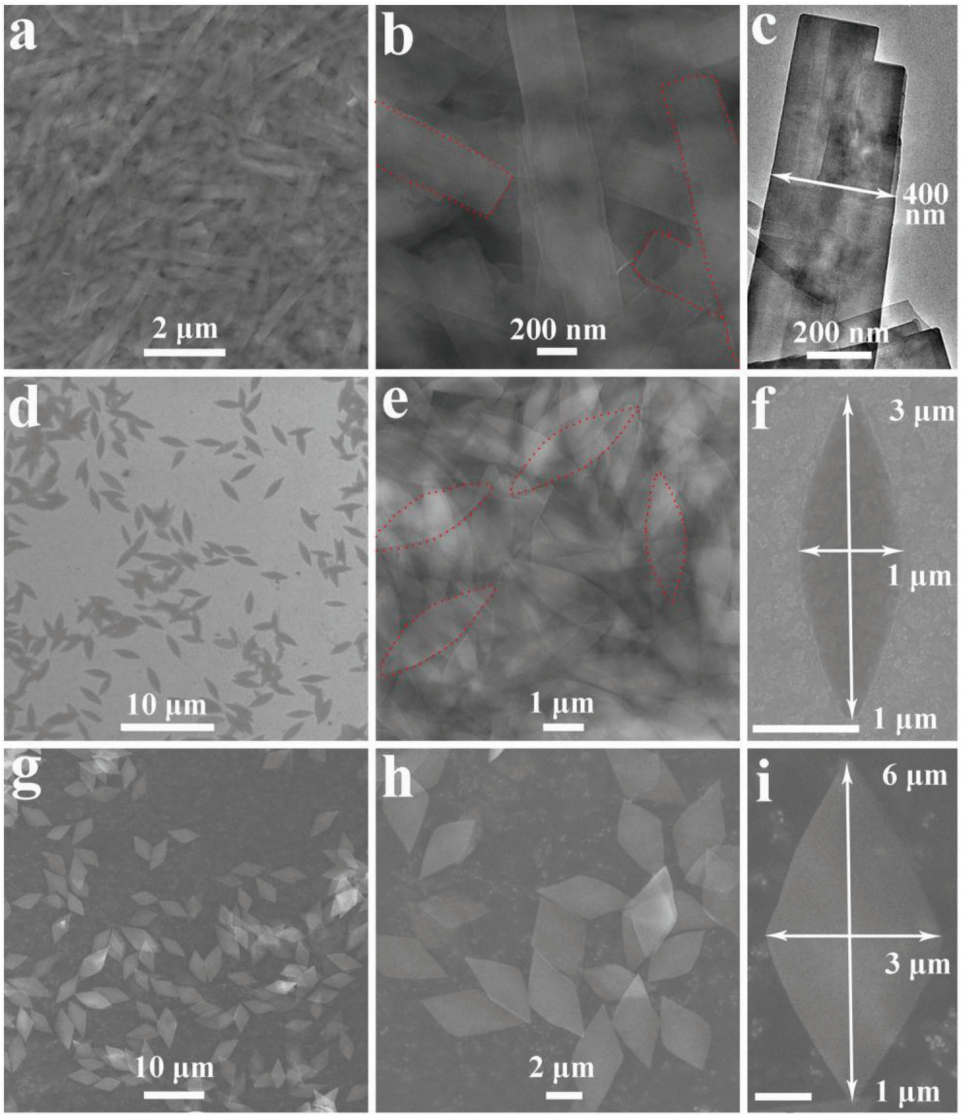

Figure 2. a,b) SEM and c) TEM images of CoPPi nanobelts, SEM images of d–f) CoPPi nanoleaves and g–i) nanorhombuses.

of $Na_4P_2O_7$:$Co(CH_3COO)_2$ is 3:2 in all above systems, and the morphology of CoPPi changes when tuning the concentration of precursors probably relates to the residual $Na_4P_2O_7$ in solution.

Besides the concentration, we also studied the influence of molar ratio between the two precursors on the morphology and crystal size control. Taking the formation of CoPPi nanobelts as an example, when the sum concentrations of the two precursors are fixed at 20% of that for preparing the nanowires and a low molar ratio of 1:4 ($Na_4P_2O_7$:$Co(CH_3COO)_2$ = 1:4) is used, few nanosheet-like structures are obtained (Figure 3b). At a higher molar ratio of 1:2 (the theoretical ratio based on chemical formula, $Co_2P_2O_7$), the size of nanosheets increased obviously (Figure 3c), and no belt-like structures are observed. When a further higher molar ratio of 3:2 is adopted and $P_2O_7^{4-}$ excessively present in the system, uniform nanobelts are formed as shown in Figure 2a,b. As the molar ratio is increased to 3:1, belt-like structures are reserved (Figure 3d). Based on the results, we can conclude that excess $P_2O_7^{4-}$ in the system is helpful for building the belt-like structure.

For better understanding the mechanism of morphology control, the crystal structure of $Co_2P_2O_7$ (ICSD No. 59291) is presented in Figure 3e, with one layer of Co^{2+} and one layer of PO_4 tetrahedra distributed alternately. In a reaction system presenting large amount of Co^{2+} (such as the ratio of 1: 4), once crystal nuclei are formed, the $P_2O_7^{4-}$ is exhausted quickly and the surface of crystal nuclei will be surrounded by the partial positively charged (δ^+) Co^{2+} (Figure 3f). This will prevent nuclei growth from generating big crystal because of the electrostatic repulsion.[33] In another case, excess of partial negatively charged (δ^-) $P_2O_7^{4-}$ ion exists in the system (such as the ratio of 3: 2). The $P_2O_7^{4-}$ will preferentially adsorb on $Co_2P_2O_7$ nuclei surface in *c*-direction (Figure 3g) when there is more Co^{2+} exposures than the other directions (Figure S6, Supporting Information), consequently suppressing the crystal growth in this orientation during crystal growth process.[29,34]

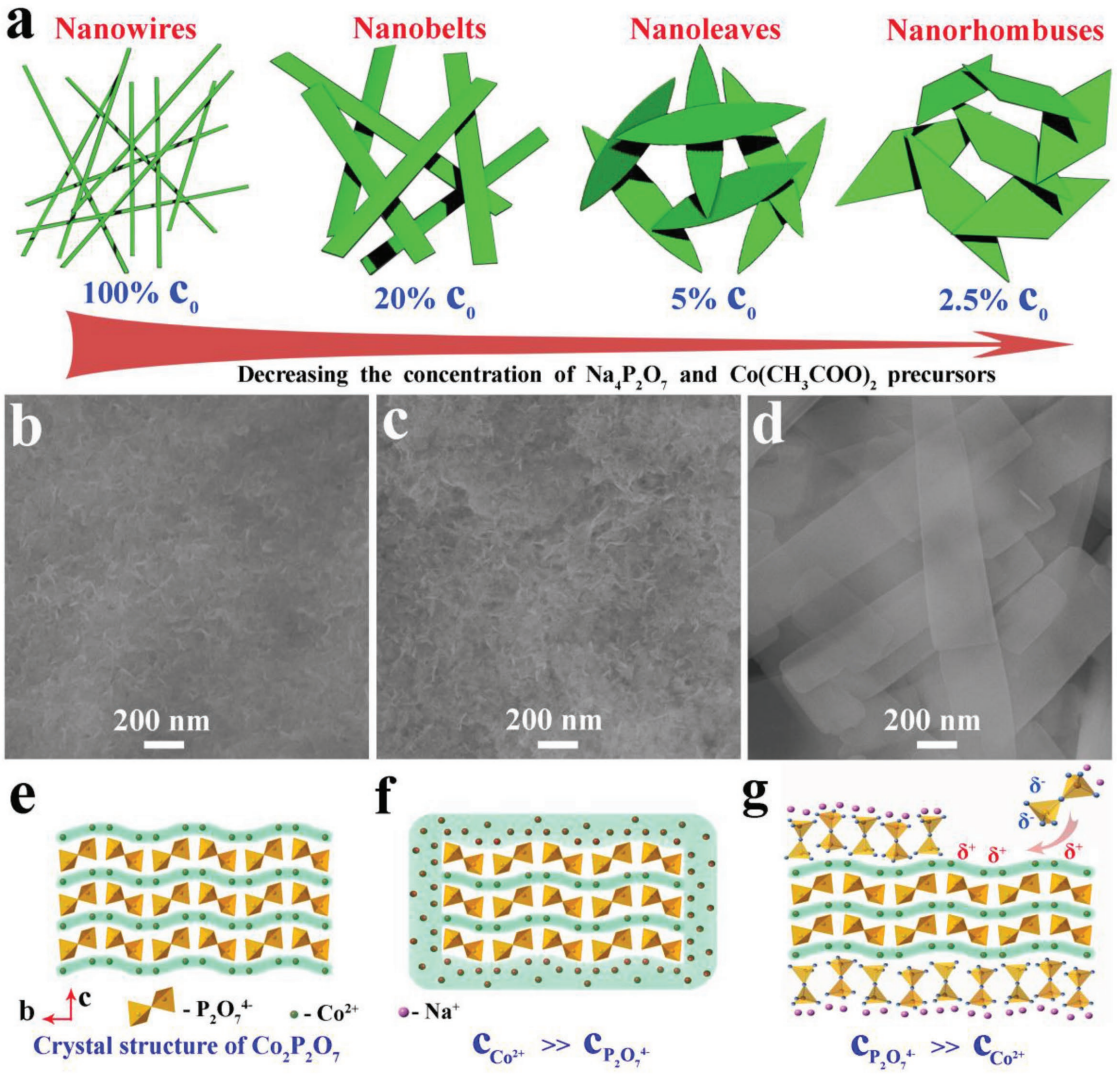

Figure 3. a) Overall scheme of precursors' concentration and structure evolution of CoPPi (C_0 is the typical concentration for preparing CoPPi nanowires, i.e., 300×10^{-3} M $Na_4P_2O_7$ and 200×10^{-3} M $Co(CH_3COO)_2$). SEM images of CoPPi prepared in ratio of b) 1:4, c) 1:2, and d) 3:1. e) Crystal structure of CoPPi, and nuclei growth in the presence of excess f) $Co(CH_3COO)_2$ and g) $Na_4P_2O_7$.

As a result, CoPPi nanobelts with large size and ultrathin thickness are produced. The $Na_4P_2O_7$ in the system not only serves as reactant for the synthesis of CoPPi but also acts as surfactant functioning as the morphology controller. Therefore, the existence of excessive $Na_4P_2O_7$ is indispensable for fabrication of CoPPi nanobelts. At a molar ratio of 3:2, as discussed above, CoPPi nanowires, nanobelts, nanoleaves, and nanorhombuses are sequentially obtained when reducing the concentration of precursor solution. Though we maintain the molar ratio when decreasing the concentration, the residual $Na_4P_2O_7$ which function as surfactant also decreases the concentration undoubtedly. Therefore, the interaction between the nuclei and surfactant will be changed and further affects the morphology of the final product.[35] The concentration of the residual $Na_4P_2O_7$ is responsible for the formation of CoPPi with different morphologies. We also prepared zinc pyrophosphate and manganese pyrophosphates with various molar ratio of starting material (for details, please see the Supporting Information). Both zinc pyrophosphate (Figure S7, Supporting Information) and manganese pyrophosphate (Figure S8, Supporting Information) show similar morphology evolution trends as that for CoPPi when raising the molar ratio. Only under a high molar ratio condition, where $P_2O_7^{4-}$ excessively exists in solution and serves as surfactant, zinc pyrophosphate and manganese pyrophosphate nanobelts can be achieved. These results suggest that the mechanism proposed above also works perfectly for the synthesis of other transition metal pyrophosphate with effective control of morphology and crystal size. This finding is of importance due to its demonstration of a great progress in nanomaterial research and design.

The electrocatalytic activities of the CoPPi nanostructures for OER were studied by a standard three-electrode setup with 1 M KOH solution as the electrolyte. All potentials reported here were measured against the SCE reference electrode and converted to reversible hydrogen electrode (RHE) potential according to the Nernst equation. For comparison, the

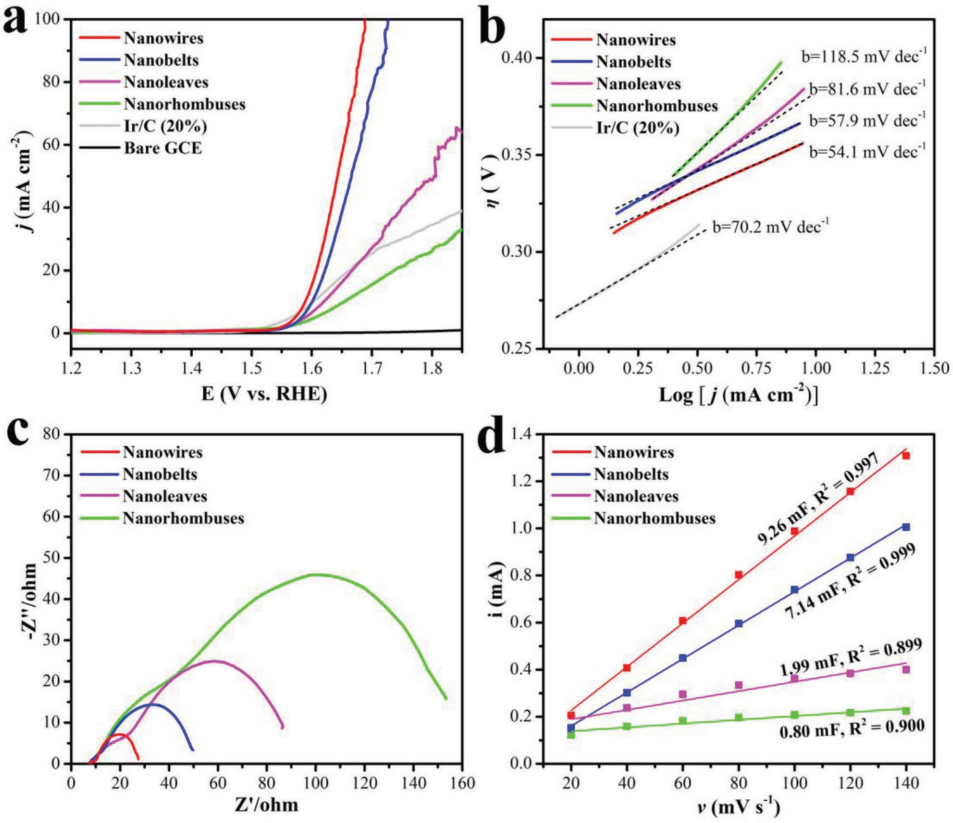

Figure 4. a) Polarization curves, b) Tafel plots, and c) Nyquist plots of CoPPi nanostructures. d) Linear plots of double-layer current ($i = 0.5 \times (i_a - i_c)$) as a function of the scan rate (ν) for CoPPi catalysts with various morphologies.

electrochemical activities of bare glassy carbon electrode (GCE) and commercial Ir/C (20%) with the same mass loading were also studied. All the electrochemical data were *iR*-compensated before further analysis. The polarization curves of CoPPi nanostructures, GCE, and Ir/C are shown in **Figure 4**a. As expected, bare GCE electrode exhibits poor OER activity. The commercial Ir/C catalyst requires an overpotential of 373 mV to deliver a current density of 10 mA cm^{-2} (η_{10}). Remarkably, CoPPi nanowires only need a very low overpotential of 359 mV at a current density of 10 mA cm^{-2}, which is much lower than that for the benchmark Ir/C catalyst, presenting the superior electrocatalytic activity for OER. The η_{10} for CoPPi nanobelts, nanoleaves, and nanorhombuses are determined to be 371, 390, and 424 mV, respectively, higher than that of nanowires. In terms of η_{10}, the catalytic performance of our CoPPi nanowires outperforms the reported coralloid $Co_2P_2O_7$ nanocrystal carbon composite catalyst CL-$Co_2P_2O_7$@C (397 mV)[19] and most of CoPi catalysts studied in alkaline media, such as mesoporous CoPi (380 mV),[36] $Co_3(PO_4)_2$ (≈430 mV),[37] and even comparable to that of CoPi@C composite, for example, CC/NPC/CP (430 mV),[38] $Co_3(PO_4)_2$@N-C (317 mV),[37] and CoPi/PCDs (350 mV).[39]

To appraise the electrocatalytic kinetics of OER, Tafel plots were obtained from the corresponding polarization curves and shown in Figure 4b. The Ir/C electrode reveals a Tafel slope of 70.2 mV dec^{-1}, comparable to the previously reported value.[40] Interestingly, CoPPi nanowires electrode exhibits a Tafel slope of 54.1 mV dec^{-1}, substantially lower than that of Ir/C, and also the CoPPi nanobelts (57.9 mV dec^{-1}), nanoleaves (81.6 mV dec^{-1}), and nanorhombuses (118.5 mV dec^{-1}), suggesting the favorable OER kinetics of CoPPi nanowires.[41] Note that this value is lower than the reported CL-$Co_2P_2O_7$@C (70 mV dec^{-1})[19] and the other CoPi based catalysts, for example, mesoporous CoPi (58.7 mV dec^{-1}),[36] $Co_3(PO_4)_2$@N-C (62 mV dec^{-1}),[37] and CC/NPC/CP (80 mV dec^{-1}).[38] In order to estimate the intrinsic activity, turnover frequency (TOF) was calculated by assuming that all catalysts were involved in OER processes (see the Supporting Information).[42] Under an overpotential of 400 mV, a TOF of 0.058 s^{-1} is achieved for CoPPi nanowires. Although the value is slightly lower than the benchmark Ir/C catalyst (0.073 s^{-1}), it is still superior to that of CoPPi nanobelts (0.038 s^{-1}), nanoleaves (0.018 s^{-1}), and nanorhombuses (0.011 s^{-1}). These results demonstrate the higher intrinsic OER activity of CoPPi nanowires compared to the other CoPPi nanostructures.

Electrochemical impedance spectroscopy (EIS) measurements were carried out to further study the electrocatalytic behaviors of CoPPi nanostructures. Nyquist plots in Figure 4c show that all the electrodes have well-defined semicircles, which correspond to charge transfer resistance (R_{ct}) in the electrochemical reaction.[43] Under a static overpotential of 375 mV, the R_{ct} of CoPPi nanowires, nanobelts, nanoleaves, and nanorhombuses are determined to be 17.6, 37.7, 70.1, and 126.1 Ω, respectively. The lowest R_{ct} of CoPPi nanowires

electrode indicates the fastest charge transfer kinetics with respect to the other nanostructures, which could be responsible for its superior OER catalytic activity. Furthermore, a potential range where no obvious Faradaic processes occur is chosen as the potential window (1.3–1.4 V) to determine the double-layer capacitance (C_{dl}) at various scan rates (Figures S9 and S10, Supporting Information). The electrochemical surface area (ECSA) and roughness factor (RF) are calculated from the corresponding C_{dl} (see the Supporting Information).[44] Figure 4d shows the double-layer charging current (i) as a function of scan rate (v) plots of CoPPi catalysts, the slope of which is C_{dl}.[44] The C_{dl} for CoPPi nanowires, nanobelts, nanoleaves, and nanorhombuses are determined to be 9.26, 7.14, 1.99, and 0.80 mF, respectively. Considering the specific capacitance (C_s) of a planar electrode, ECSA for CoPPi nanowires is thus calculated to be 231.5 cm^2. The ECSA of CoPPi nanowires is higher than CoPPi nanobelts (178.5 cm^2), nanoleaves (49.8 cm^2), and nanorhombuses (20.0 cm^2). RF is then calculated by dividing ECSA with the geometric area of the electrode. Accordingly, the RF is determined to be 1837.3 for CoPPi nanowires, 1416.7 for nanobelts, 395.2 for nanoleaves, and 158.7 for nanorhombuses. CoPPi nanowires exhibit the highest surface area and roughness among other nanostructures, which would benefit the OER for exposure of more catalytic reactive site. The corresponding electrochemical parameters of CoPPi catalysts with various morphologies are summarized in Table S1 (Supporting Information) for better comparison. As shown in Figures 1 and 2, the crystal size of CoPPi materials increases rapidly from nanowires to nanorhombuses, leading to the decreasing in ECSA and RF but raising in R_{ct}. Since OER occurs at the interfaces between the electrode material and the electrolyte, the changes of ECSA, RF, and R_{ct} will definitely affect the OER activity of the electrocatalyst accordingly. As a result, from CoPPi nanowires to CoPPi nanorhombuses the values of Tafel slope and η_{j10} increased dramatically but the TOF values decreased, these trends suggest the OER process becomes more and more unfavorable.

It is very interesting to observe that OER catalytic activities of CoPPi nanowires are higher than other CoPPi nanostructures due to the larger surface area, lower Faraday resistance, and higher mass transport. This can be more fundamentally explained. The larger surface area is mainly resulted from the larger aspect ratio of the nanowires,[45] while the fast charge transport along one dimension and the reactant easy access to its surface can definitely enhance the charge transfer rate.[45b,46] In addition, the diffusion model of both reactant and product for a nanowire such as CoPPi nanowires is a radial diffusion one, a 2D diffusion process, which has much faster mass transport rate than a 1D diffusion process occurring on a 2D structured electrode surface such as nanobelts, nanoleaves, and nanorhombuses of CoPPi. The 1D CoPPi nanowires can also offer higher specific pore volume[47] when compared to others and the voids between the nanowires could render short paths for mass transport. This is why the CoPPi nanowires can simultaneously boost charge transfer and mass transport for high electrocatalytic activities.

For practical applications, we further investigated the stability of CoPPi nanowires catalyst. Continuous cyclic voltammetry (CV) cycling test was performed over a range of 1.3–1.7 V at a scan rate of 100 mV s^{-1}. Compared to the initial curves, the polarization curve after 5000 cycles shows the same feature with no change of the current density (**Figure 5**a). On the other hand, a chronoamperometric curve of CoPPi nanowires was acquired at a static potential of 1.63 V (η = 400 mV). After a long period of 10 h OER operating test, the electrode preserves up to 92% of its original OER current (Figure 5b), demonstrating a good stability of CoPPi nanowires. It is noted that there is a sudden drop of the OER current at ≈7 h. This is mainly resulted from the generated oxygen bubbles occasionally absorbed on the electrode surface. The high activity, superior stability, and low cost of CoPPi nanowires make it a promising candidate to substitute the noble-based electrocatalyst for large-scale application in water electrolysis.

In summary, we have developed a new and facile strategy for morphology-controllable synthesis of CoPPi nanostructures without any surfactant and additives. By tuning the concentration and ratio of precursor solutions, CoPPi nanomaterials with various morphologies are obtained. We find that $Na_4P_2O_7$ acts as both reactant and pseudo-surfactant to achieve various unique nanostructures. A detailed mechanism is proposed, which can be used for morphology-controllable synthesis of other transition metal pyrophosphates thus offering universal significance

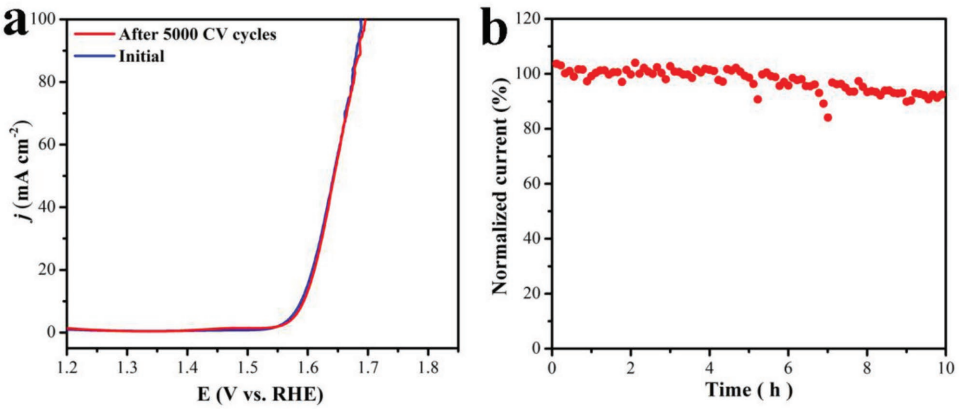

Figure 5. a) Polarization curves of CoPPi nanowires acquired before and after 5000 CV cycles, and b) chronoamperometric curve recorded under a static potential of 1.63 V for 10 h.

and demonstrating a great progress in nanomaterial research and design. Among all CoPPi nanostructures, CoPPi nanowires exhibit the best catalytic performance toward OER. The low cost, unique nanostructure, high electrocatalytic activity, and superior stability hold great promises for CoPPi nanowires becoming broad applications with industrial hydrogen production via water electrolysis.

Supporting Information

Supporting Information is available from the Wiley Online Library or from the author.

Acknowledgements

This work was supported by MOE Tier 1 (RG19/17) and (RG22/16). The authors also gratefully acknowledge the financial support from the Institute for Clean Energy and Advanced Materials (Southwest University, Chongqing, China); the Start-up grant under SWU111071 from the Southwest University (Chongqing, China); the Chongqing Science and Technology Commission (cstc2017jcyjAX0199); and Graduate Student Research Innovation Project of Chongqing (CYB16055).

Conflict of Interest

The authors declare no conflict of interest.

Keywords

cobalt pyrophosphate, electrocatalysis, morphology control, nanowires, oxygen evolution reaction

Received: March 19, 2018
Revised: May 18, 2018
Published online: July 2, 2018

[1] a) K. Zeng, D. Zhang, *Prog. Energy Combust. Sci.* **2010**, *36*, 307; b) T. N. Huan, G. Rousse, S. Zanna, I. T. Lucas, X. Xu, N. Menguy, V. Mougel, M. Fontecave, *Angew. Chem., Int. Ed.* **2017**, *56*, 4792; c) W. Ai, W. Zhou, Z. Du, Y. Du, H. Zhang, X. Jia, L. Xie, M. Yi, T. Yu, W. Huang, *J. Mater. Chem.* **2012**, *22*, 23439.

[2] a) J. A. Turner, *Science* **2004**, *305*, 972; b) J. X. Feng, S. H. Ye, H. Xu, Y. X. Tong, G. R. Li, *Adv. Mater.* **2016**, *28*, 4698.

[3] L. Davidson, R. A. Stebbins, *Serious Leisure and Nature*, Springer, Berlin **2011**, p. 57.

[4] Y. Jin, H. Wang, J. Li, X. Yue, Y. Han, P. K. Shen, Y. Cui, *Adv. Mater.* **2016**, *28*, 3785.

[5] a) C. Guo, Y. Zheng, J. Ran, F. Xie, M. Jaroniec, S.-Z. Qiao, *Angew. Chem., Int. Ed.* **2017**, *56*, 8539; b) J. X. Feng, H. Xu, Y. T. Dong, S. H. Ye, Y. X. Tong, G. R. Li, *Angew. Chem., Int. Ed.* **2016**, *55*, 3694.

[6] X. F. Lu, L. F. Gu, J. W. Wang, J. X. Wu, P. Q. Liao, G. R. Li, *Adv. Mater.* **2017**, *29*, 1604437.

[7] a) L. C. Seitz, C. F. Dickens, K. Nishio, Y. Hikita, J. Montoya, A. Doyle, C. Kirk, A. Vojvodic, H. Y. Hwang, J. K. Norskov, *Science* **2016**, *353*, 1011; b) S. H. Ye, Z. X. Shi, J. X. Feng, Y. X. Tong, G. R. Li, *Angew. Chem., Int. Ed.* **2018**, *57*, 2672.

[8] A. Sivanantham, P. Ganesan, S. Shanmugam, *Adv. Funct. Mater.* **2016**, *26*, 4661.

[9] N.-T. Suen, S.-F. Hung, Q. Quan, N. Zhang, Y.-J. Xu, H. M. Chen, *Chem. Soc. Rev.* **2017**, *46*, 337.

[10] a) P. Du, R. Eisenberg, *Energy Environ. Sci.* **2012**, *5*, 6012; b) L. Han, S. Dong, E. Wang, *Adv. Mater.* **2016**, *28*, 9266.

[11] J. Wang, W. Cui, Q. Liu, Z. Xing, A. M. Asiri, X. Sun, *Adv. Mater.* **2016**, *28*, 215.

[12] a) S. Mao, Z. Wen, T. Huang, Y. Hou, J. Chen, *Energy Environ. Sci.* **2014**, *7*, 609; b) F. Song, X. Hu, *J. Am. Chem. Soc.* **2014**, *136*, 16481.

[13] H. Senchuan, M. Yuying, H. Shiman, G. Anandarup, W. Qili, L. Junhao, T. Shengfu, A. Tewodros, W. Mingmei, *Adv. Funct. Mater.* **2017**, *27*, 1606585.

[14] Y. P. Zhu, Y. P. Liu, T. Z. Ren, Z. Y. Yuan, *Adv. Funct. Mater.* **2015**, *25*, 7337.

[15] a) P. Chen, K. Xu, Z. Fang, Y. Tong, J. Wu, X. Lu, X. Peng, H. Ding, C. Wu, Y. Xie, *Angew. Chem.* **2015**, *127*, 14923; b) Y. Zhang, B. Ouyang, J. Xu, G. Jia, S. Chen, R. S. Rawat, H. J. Fan, *Angew. Chem., Int. Ed.* **2016**, *55*, 8670.

[16] M. W. Kanan, D. G. Nocera, *Science* **2008**, *321*, 1072.

[17] D. A. Lutterman, Y. Surendranath, D. G. Nocera, *J. Am. Chem. Soc.* **2009**, *131*, 3838.

[18] K. M. S. Etheredge, S.-J. Hwu, *Inorg. Chem.* **1995**, *34*, 1495.

[19] Y. Chang, N.-E. Shi, S. Zhao, D. Xu, C. Liu, Y.-J. Tang, Z. Dai, Y.-Q. Lan, M. Han, J. Bao, *ACS Appl. Mater. Interfaces* **2016**, *8*, 22534.

[20] a) P. Barpanda, M. Avdeev, C. D. Ling, J. Lu, A. Yamada, *Inorg. Chem.* **2013**, *52*, 395; b) M. Tamaru, S. C. Chung, D. Shimizu, S.-i. Nishimura, A. Yamada, *Chem. Mater.* **2013**, *25*, 2538; c) Z. Khan, B. Senthilkumar, S. Lim, R. Shanker, Y. Kim, H. Ko, *Adv. Mater. Interfaces* **2017**, *4*, 1700059.

[21] C. Chen, N. Zhang, Y. He, B. Liang, R. Ma, X. Liu, *ACS Appl. Mater. Interfaces* **2016**, *8*, 23114.

[22] A. S. Aricò, P. Bruce, B. Scrosati, J.-M. Tarascon, W. Van Schalkwijk, *Nat. Mater.* **2005**, *4*, 366.

[23] M. Harcharras, A. Ennaciri, F. Capitelli, G. Mattei, *Vib. Spectrosc.* **2003**, *33*, 189.

[24] X. Ren, R. Ge, Y. Zhang, D. Liu, D. Wu, X. Sun, B. Du, Q. Wei, *J. Mater. Chem. A* **2017**, *5*, 7291.

[25] T. J. Chuang, C. R. Brundle, D. W. Rice, *Surf. Sci.* **1976**, *59*, 413.

[26] Y. Du, X. Zhu, X. Zhou, L. Hu, Z. Dai, J. Bao, *J. Mater. Chem. A* **2015**, *3*, 6787.

[27] M. T. Rinke, H. Eckert, *Phys. Chem. Chem. Phys.* **2011**, *13*, 6552.

[28] R. V. Siriwardane, *Langmuir* **1991**, *7*, 497.

[29] Y. Sun, B. Mayers, T. Herricks, Y. Xia, *Nano Lett.* **2003**, *3*, 955.

[30] C. Wang, Y. Hu, C. M. Lieber, S. Sun, *J. Am. Chem. Soc.* **2008**, *130*, 8902.

[31] T. Yu, D. Y. Kim, H. Zhang, Y. Xia, *Angew. Chem.* **2011**, *123*, 2825.

[32] a) V. K. LaMer, R. H. Dinegar, *J. Am. Chem. Soc.* **1950**, *72*, 4847; b) R. Viswanatha, D. Sarma, *Nanomaterials Chemistry: Recent Developments and New Directions*, Wiley-VCH, Weinheim **2007**, p. 139.

[33] N. Goldstein, L. F. Greenlee, *J. Nanopart. Res.* **2012**, *14*, 760.

[34] B. Wiley, Y. Sun, B. Mayers, Y. Xia, *Chem. - Eur. J.* **2005**, *11*, 454.

[35] Q. Chen, G. Du, Y. Dong, Z. Cao, Z. Xie, L. Zheng, *Sci. Bull.* **2017**, *62*, 1359.

[36] M. Pramanik, C. Li, M. Imura, V. Malgras, Y.-M. Kang, Y. Yamauchi, *Small* **2016**, *12*, 1709.

[37] C.-Z. Yuan, Y.-F. Jiang, Z. Wang, X. Xie, Z.-K. Yang, A. B. Yousaf, A.-W. Xu, *J. Mater. Chem. A* **2016**, *4*, 8155.

[38] Z. Cai, W. Xu, F. Li, Q. Yao, X. Chen, *ACS Sustainable Chem. Eng.* **2017**, *5*, 571.

[39] S. Zhao, C. Li, H. Huang, Y. Liu, Z. Kang, *J. Materiomics* **2015**, *1*, 236.

[40] L. Fu, P. Cai, G. Cheng, W. Luo, *Sustainable Energy Fuels* **2017**, *1*, 1199.

[41] Y. Tong, P. Chen, T. Zhou, K. Xu, W. Chu, C. Wu, Y. Xie, *Angew. Chem., Int. Ed.* **2017**, *56*, 7121.
[42] X. Lu, C. Zhao, *Nat. Commun.* **2015**, *6*, 6616.
[43] C. X. Guo, L. Y. Zhang, J. Miao, J. Zhang, C. M. Li, *Adv. Energy Mater.* **2013**, *3*, 167.
[44] C. C. McCrory, S. Jung, J. C. Peters, T. F. Jaramillo, *J. Am. Chem. Soc.* **2013**, *135*, 16977.
[45] a) Z. Tong, S. Liu, X. Li, J. Zhao, Y. Li, *Nanoscale Horiz.* **2018**, *3*, 261; b) M. S. Park, G. X. Wang, Y. M. Kang, D. Wexler, S. X. Dou, H. K. Liu, *Angew. Chem., Int. Ed.* **2007**, *46*, 750.
[46] L. Yi, Y. Liu, N. Yang, Z. Tang, H. Zhao, G. Ma, Z. Su, D. Wang, *Energy Environ. Sci.* **2013**, *6*, 835.
[47] B. Weng, S. Liu, Z.-R. Tang, Y.-J. Xu, *RSC Adv.* **2014**, *4*, 12685.